Bian, Y. Q., Nix, A. R., Tameh, E. K., & McGeehan, J. P. (2008). MIMO-OFDM WLAN architectures, area coverage, and link adaptation for urban hotspots. IEEE Transactions on Vehicular Technology, 57(4), 2364 - 2374. 10.1109/TVT.2007.909289

MIMO–OFDM WLAN Architectures, Area Coverage, and Link Adaptation for Urban Hotspots

Yan Q. Bian, Andrew R. Nix, Eustace K. Tameh, and Joseph P. McGeehan

***Abstract*—This paper considers the suitability of a range of multi-input–multi-output (MIMO) orthogonal frequency-division multiplexing architectures for use in urban hotspots. A ray-tracing propagation model is used to produce realistic MIMO channel data. This information is used to determine the expected throughput and area coverage for various physical (PHY) layer schemes. Site-specific throughput predictions are generated in a city-center environment. Link adaptation (LA) is shown to play a key role in the choice of space–time algorithm, the use of adaptive modulation and coding, and the number of antennas employed at both ends of the radio link. No single PHY layer scheme is suitable to cover the entire coverage area. Results demonstrate the need for MIMO LA under a wide range of channel conditions. For the area under test, 2% of covered locations selected a spatial multiplexing (SM) scheme, 50% selected a space–time block coding (STBC) scheme, and 48% selected a hybrid SM/STBC scheme. With suitable power control and LA, for the scenario under consideration, high peak capacities and good geographic coverage were achieved.**

***Index Terms*—Link adaptation (LA), orthogonal frequency-division multiplexing (OFDM), power control, propagation, space–time block codes (STBCs), spatial multiplexing (SM).**

I. Introduction

SPECTRUM predictions for future cellular networks indicate large shortfalls by 2010, if not beforehand [1]. This increasingly crowded spectrum means that new channels are rarely available and that future demand must be met by deploying more spectrally efficient wireless technologies. It is well reported that multi-input–multi-output (MIMO) physical (PHY) layer techniques have the potential to significantly increase bandwidth efficiency based on the premise that operation occurs in a rich-scattering environment [2]. Coded orthogonal frequency-division multiplexing (COFDM) is also a well-established technique for achieving low-cost broadband wireless connectivity [3]. COFDM has been chosen as the air interface for a range of new standards [4], [5], including IEEE 802.11 and IEEE 802.16. The ideas of MIMO and OFDM have been combined in a number of papers to form a new class of MIMO–OFDM system [6], [7]. MIMO–OFDM is commonly used to simplify the extension of MIMO to a wideband channel (since traditional narrowband analyses can be trivially extended to support higher data rates). MIMO–OFDM is a promising candidate for hotspot (802.11n) and urban last-mile (802.16) applications. Any practical solution must do the following: 1) effectively share the limited spectral resource; 2) provide reliable quality-of-service (QoS) throughout the coverage area; 3) reduce transmit power levels and terminal power consumption; and 4) minimize the cost of the access point (AP) and mobile stations (MS).

The radio propagation characteristics in an outdoor environment result in space-selective fading. Spatial correlation between subchannels in the MIMO channel matrix limits the level of spectral efficiency that can be achieved in practice. Performance is a function of parameters such as the K-factor, the spread in the angles of departure (AoD) and the angles of arrival (AoA), the antenna-element separations, the delay spread (DS), and the signal-to-noise ratio (SNR) [8], [9]. The theoretic MIMO capacity can be predicted by passing the channel data into the Foschini capacity equation [10], [11]. In [11], the impact of perfect transmitter power control (TPC) was considered (i.e., no upper transmit power limit was applied). In addition to spatial correlation, the achievable peak capacity for a practical system strongly depends on the PHY layer configuration. The choice of channel coding scheme, modulation strategy, space–time processing algorithm, and detection technique all influence the capacity and QoS achieved. Higher order modulation schemes will increase the link throughput but require a higher SNR to achieve a low packet error rate (PER). Space–time block codes (STBCs) provide a strong diversity gain (which is desirable at a low SNR) but cannot increase the link throughput without the use of adaptive modulation and coding (AMC) [9]. Previous work has already considered the application of adaptive MIMO [12]–[16].

This paper combines channel and link-level simulators to evaluate the performance of different MIMO–OFDM schemes in realistic correlated channels. Statistical results are provided for each scheme in an example outdoor hotspot. Channel modeling is based on ray tracing, where the mobile transitions from line-of-sight (LoS) to non-line-of-sight (NLoS) are naturally handled by the algorithms. Design guidelines are provided for MIMO systems that combine high throughput with good area coverage in an urban environment.

The paper is organized as follows: Section II introduces two MIMO $\mathbf{H}$-matrix models, the first being a statistical parameter-based model, and the second being a ray-tracing

Manuscript received January 18, 2006; revised May 3, 2007 and August 7, 2007. This work was supported by Toshiba Research Europe Ltd., Bristol, U.K. The review of this paper was coordinated by Dr. K. Dandekar.

Y. Q. Bian is with the Centre for Communications Research, University of Bristol, BS8 1UB Bristol, U.K. (e-mail: y.q.bian@bristol.ac.uk).

A. R. Nix is with the University of Bristol, BS8 1UB Bristol, U.K. (e-mail: andy.nix@bristol.ac.uk).

E. K. Tameh was with the University of Bristol, BS8 1UB Bristol, U.K. He is now with ProVision Communication Technologies Ltd., BS4 4EU Bristol, U.K. (e-mail: eustace.tameh@provision-comm.com).

J. P. McGeehan is with the University of Bristol, BS8 1UB Bristol, U.K., and also with Toshiba Research Europe Ltd., BS1 4ND Bristol, U.K. (e-mail: joe.mcgeehan@toshiba-trel.com).

Color versions of one or more of the figures in this paper are available online at http://ieeexplore.ieee.org.

Digital Object Identifier 10.1109/TVT.2007.909289

deterministic (RTD) model. The limitations and assumptions of the TGn802.11n MIMO channel model [17] are summarized, and an alternative approach is defined based on the site-specific output from the RTD model. This approach is shown to have a number of key advantages for use in coverage and link adaptation (LA) studies. Section III describes the process of capacity prediction using the ray-tracing propagation model. In Section IV, the use of dynamic transmit power control (DTPC) is presented. Section V describes the space–time methods used in this paper and explains the role of LA in the context of MIMO–OFDM. Section VI presents a range of simulation results, with conclusions given in Section VII.

II. MIMO Channel Modeling

A. TGn802.11n Channel Model

The TGn802.11n channel models (models A–F) were developed by the IEEE for evaluating multiantenna-element wireless local area network (WLAN) systems [17]. Models E and F represent large open areas (root mean square (rms) DS of 100 and 150 ns, respectively) and, hence, are the most appropriate for the hotspots considered in this paper. The models are based on multipath clusters, and the method follows the MIMO modeling approach presented in [18] and [19], which utilizes receive and transmit covariance matrices. The MIMO $\mathbf{H}$-matrix for the lth tap in the channel impulse response (CIR) is separated into a fixed LoS matrix $\mathbf{H}_{\mathrm{LoS}}$ and a Rayleigh NLoS matrix $\mathbf{H}_{\mathrm{Rayleigh}}$ [20] and can be expressed as

$$\mathbf{H}_l = \sqrt{P_l}\left(\sqrt{\frac{K}{1+K}}\begin{bmatrix} e^{j(\varphi+\Delta\phi_{1,1})} & \cdots & e^{j(\varphi+\Delta\phi_{1,N_T})} \\ \vdots & \ddots & \vdots \\ e^{j(\varphi+\Delta\phi_{N_R,1})} & \cdots & e^{j(\varphi+\Delta\phi_{N_R,N_T})} \end{bmatrix} + \sqrt{\frac{1}{1+K}}\begin{bmatrix} X_{1,1} & \cdots & X_{1,N_T} \\ \vdots & \ddots & \vdots \\ X_{N_R,1} & \cdots & X_{N_R,N_T} \end{bmatrix}\right) \quad (1)$$

where N_T, N_R, K, and P_l represent the number of transmit and receive antennas, the Ricean K-factor, and the power of the lth tap, respectively. The channel matrix is normalized such that $\|\mathbf{H}_l\|^2 = N_T N_R P_l$. The terms $e^{j(\varphi+\Delta\phi_{n,m})}$ and $X_{n,m}$ represent elements of $\mathbf{H}_{\mathrm{LoS}}$ and $\mathbf{H}_{\mathrm{Rayleigh}}$, respectively, for the nth receiving and mth transmitting antenna. For the LoS ray, φ and $\Delta\phi_{n,m}$, respectively, denote the initial reference phase (based on a point-source evaluation of the link from Tx element 1 to Rx element 1) and the relative phase difference that results between the mth transmit antenna and the nth receive antenna. If we assume N_T transmit antennas and N_R receive antennas configured in the form of a regularly spaced (horizontally orientated) uniform linear array (ULA), then we can write

$$\Delta\phi_{n,m} = 2\pi(m-1)\frac{d}{\lambda}\sin(\alpha_{\mathrm{LoS,tx}}) + 2\pi(n-1)\frac{d}{\lambda}\sin(\pi-\alpha_{\mathrm{LoS,rx}}) \quad (2)$$

where λ, d, $\alpha_{\mathrm{LoS,tx}}$, and $\alpha_{\mathrm{LoS,rx}}$ represent the wavelength, the interelement separation distance, the AoD, and the AoA of the LoS ray, respectively. The $\mathbf{H}_{\mathrm{Rayleigh}}$ term for a single narrowband spatially correlated channel uses a "Kronecker" structure, as described in [17].

Several assumptions are made in the TGn802.11n channel model, which include the following: 1) The K-factor is only modeled for the first tap, and all remaining taps in the cluster follow Rayleigh-distributed random variables with a mean square value that obeys a double exponential decay law; 2) the mean AoA/AoD values are assigned to each cluster based on uniform random variables in the range $[0-2\pi]$; 3) the impact of elevation spread is ignored, and thus, antenna array orientation is restricted to the horizontal plane; 4) the azimuth power angle spectrum (PAS) is assumed to follow a Laplacian distribution; 5) the cluster rms DS and rms angle spread (AS) is modeled using correlated lognormal random variables; and 6) polarization is addressed by assigning a cross-polar discrimination value of 10 dB for the fixed $\mathbf{H}_{\mathrm{LoS}}$ matrix and 3 dB for the variable $\mathbf{H}_{\mathrm{Rayleigh}}$ matrix. It was shown in [21]–[24] that the "Kronecker" structure does not always produce channels that agree well with measured capacity.

B. RTD Model

Unlike the parameter-based TGn802.11n model discussed in Section II-A, the use of ray tracing provides accurate estimates for parameters such as the PAS at both ends of the link and the CIR for each antenna link (without the need for specific assumptions). Previous work has shown that ray tracing can accurately predict the detailed correlation structure in a MIMO channel [25]. Within the RTD model, electromagnetic waves are traced in 3-D space from the transmitter to the receiver, together with building, edge, corner, and terrain interactions. It requires geographic data in the form of terrain, building, foliage, and ground cover type and was previously validated using measurement data collected in mixed urban and rural environments [26].

For the RTD model, MIMO $\mathbf{H}$-matrices are fully determined from the point-source predicted multipath components (MPCs) linking the AP to each MS location. The model provides information on the amplitude, phase, time delay, AoA, and AoD of each MPC. From the resulting ensemble set of components, and given the array geometries, it is possible to expand this point-source single-input–single-output (SISO) data to derive a representative set of MIMO channel data, as shown in Fig. 1. It should be noted that the model does not take into account the pattern diversity [27], [28] created by antenna elements in the near field. The MIMO $\mathbf{H}$-matrices are determined using the following procedure.

1) Perform point-source ray tracing from the AP to the MS.
2) Apply a random phase to all the point-source MPCs.
3) Generate the $\mathbf{H}$-matrix for each MPC based on the $[m,n]$ array geometries.
4) Apply time binning to the $[m,n]$th $\mathbf{H}$-matrix data set (based on the system bandwidth) to generate the CIR for the $[m,n]$th link.
5) Fourier transform each CIR to generate the $[m,n]$th frequency response at each of the required OFDM subcarriers.

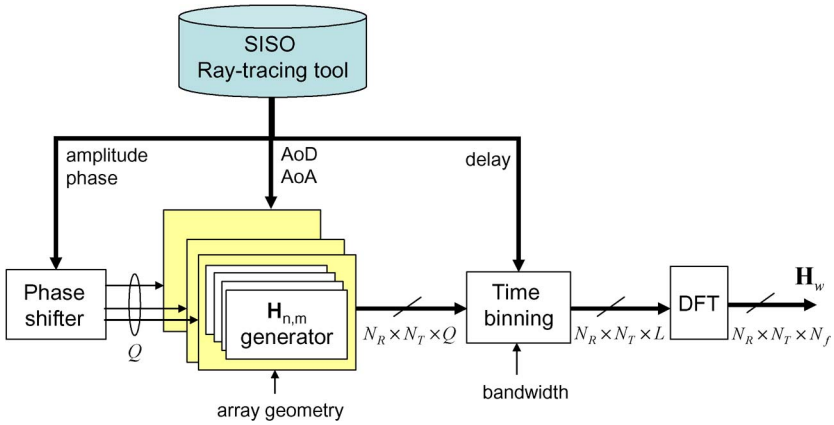

Fig. 1. RTD MIMO channel modeling.

Steps 2–5 are repeated as necessary to achieve a statistically large set of channels for PHY layer PER averaging (1000 independent channels per point are used in this study). To create an instantaneous fading channel, in step 2, a random phase shift is added to each MPC. The $\overline{\Delta\theta} = [\Delta\theta_1, \ldots, \Delta\theta_Q]$ vector comprises a set of Q independent and uniformly distributed random phases in the range $[0{-}2\pi]$, where Q represents the total number of paths traced to a given MS. The MIMO $\mathbf{H}$-matrix for the qth ray is obtained using

$$\mathbf{H}_l^q = \sqrt{P_q} \begin{bmatrix} e^{j(\varphi_q + \Delta\phi^q_{1,1} + \Delta\theta_q)} & \cdots & e^{j(\varphi_q + \Delta\phi^q_{1,N_T} + \Delta\theta_q)} \\ \vdots & \ddots & \vdots \\ e^{j(\varphi_q + \Delta\phi^q_{N_R,1} + \Delta\theta_q)} & \cdots & e^{j(\varphi_q + \Delta\phi^q_{N_R,N_T} + \Delta\theta_q)} \end{bmatrix} \tag{3}$$

where P_q and φ_q represent the ray power and the point-source predicted initial phase of the qth traced MPC, respectively. The $\Delta\phi^q_{n,m}$ terms are obtained using (2), with $\alpha_{\mathrm{LoS,rx}}$ and $\alpha_{\mathrm{LoS,tx}}$ replaced with the AoA and AoD for the qth ray, respectively. These terms expand the point-source ray analysis and enable the relative phase of each predicted MPC to be computed for each of the $[m, n]$ antenna links. To generate an $\mathbf{H}$-matrix suitable for MIMO–OFDM modeling, a system bandwidth B is employed based on the IEEE 802.11a/n standard. For high-throughput studies, a bandwidth of 40 MHz is assumed (using 128 carriers); however, for standard 802.11a/g studies, a bandwidth of 20 MHz is used. In step 4, multipaths from a given antenna link are grouped into time bins $T_s = 1/B$, which results in a CIR. The instantaneous $\mathbf{H}$-matrix in the time domain has dimensions of $N_R \times N_T \times L$, where L is the number of time taps after binning. The frequency response $\mathbf{H}_w$ is calculated from an N_f-point discrete Fourier transform of the CIR, where N_f represents the total number of subcarriers in the OFDM system. The resulting wideband $\mathbf{H}$-matrix comprises N_f narrowband $\mathbf{H}$-matrices: one for each frequency subcarrier. The spatial correlation between each MIMO link is determined by the arrival/departure angles of the predicted MPCs and the array geometry. The frequency-domain correlation (between OFDM subbands) is determined by the time-binned CIR. The channel K-factor is calculated from the CIR. Fig. 2 demonstrates that each MIMO link ($\mathbf{H}_{n,m}$) has its own individual frequency power profile at each instant in time. The figure

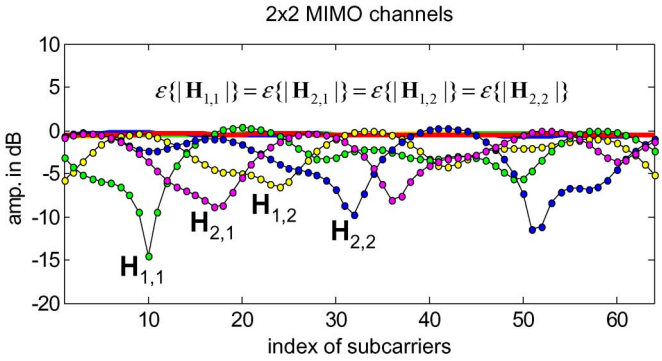

Fig. 2. Instantaneous frequency power profile of 2×2 MIMO channels.

shows that $\varepsilon\{|\mathbf{H}_{n,m}|\}$ is flat across frequency for each of the $[n, m]$ links (note that $\varepsilon\{\cdot\}$ represents the expectation function and $|\cdot|$ indicates the Frobenius norm). For each MS location, a set of wideband MIMO channels is generated for use in the PHY layer simulation. This set of channel data was generated by repeating steps 2–5, with each iteration using a different set of random phase shifts $\overline{\Delta\theta}$.

C. Suitability of MIMO Channel Model

While the parameter-based TGn802.11n model is well suited for the evaluation of MIMO PHY layer candidates, many of its underlying assumptions make the model questionable for LA and coverage studies, where transitions between environment types, K-factors, and AS/DS values are critical. For example, the inappropriate assumption on the Kronecker structure has been shown to limit MIMO system evaluation in realistic indoor environments [21]–[24]. The TGn802.11n model requires the AP and MS to be located in a similar surrounding environment. For indoor WLANs, multipath reflectors tend to be similar at the AP and MS. However, this is not the case for hotspot applications, where the AP is mounted much higher than the MS, and unlike the AP, the MS is commonly surrounded by local scatters. In particular, it should be noted that the assumption of identical PAS statistics at the Tx and Rx is not observed in our ray model (since the MS is often in a different environment type relative to the AP). Furthermore, analysis of the RTD data shows that there

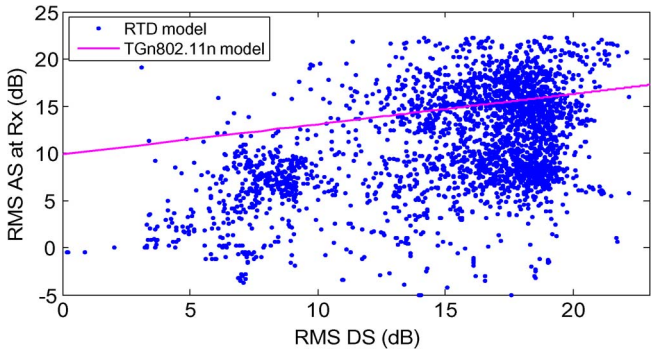

Fig. 3. Scatter plot of AS versus DS at the receiver.

is no simple relationship between the DS and the AS for a typical urban environment, as shown in Fig. 3. Here, the rms DS and rms AS are plotted as dB values using $10\log10$ (rms DS) and $10\log10$ (rms AS), respectively. Unlike the 802.11n model, the RTD model is good for site-specific performance prediction. The DS/AS dependence in the TGn802.11n model results in a large AS for models E and F (which have large DS). This produces favorable correlation statistics (in both space and frequency) for these model types. To avoid these problems, a better solution is to directly derive the entries of the MIMO channel matrix from the steering vector and the parameters [29], [30] computed through the RTD model. The power of each MPC is computed by the ray-tracing tool based on the unfolded path length and the specific reflections and diffractions present in the path. Using this approach, it is not necessary to assume or apply a statistical path loss model.

The disparity between the TGn802.11n model and our ray-traced data is at its greatest in high K-factor channels. High spatial and spectral decorrelation produces an overprediction of the MIMO capacity when the TGn802.11n channel models are applied to outdoor hotspots. Throughput results are shown in Section VI (Fig. 7). For LA studies, the accurate modeling of LoS locations (and the resulting correlations) is vital. This occurs since rank-deficient channels cannot support the high-rate spatial multiplexing (SM) schemes under test. Moreover, it is often suggested that cross-polar MIMO schemes can be used in LoS locations [17]. However, the poor modeling of polarization and the resulting correlations in the TGn802.11n model make a detailed study of this approach very difficult to perform.

To overcome the aforementioned limitations, in our LA study, the channel matrix data (which is fed to the PHY layer simulator) are directly generated from the predicted spatial and temporal MPCs, as described in Section II-B. These components are generated for each AP–MS link using our site-specific ray-tracing model. Hence, the resulting spatial and temporal correlations match more closely those seen in practice [25]. Finally, the use of predicted ray data also allows the modeling of arbitrary antenna-element geometries, patterns, and polarizations at the AP and MS.

III. MIMO Channel Capacity Prediction

To predict the theoretic MIMO capacity, among other parameters, it is necessary to compute the average received SNR. An estimate of the average received power P_{av} can be computed from a power sum of all the arriving MPCs at a given location. The average SNR is given by the following equation:

$$\text{SNR (dB)} = P_{\text{av}}\,(\text{dB}_{\text{m}}) - K_{\text{Boltzmann}}TB\,(\text{dB}_{\text{m}}) - NF\,(\text{dB}) \tag{4}$$

where $K_{\text{Boltzmann}} = 1.38 \times 10^{-20}$ mW $\cdot$ Hz^{-1} $\cdot$ K^{-1}, and P_{av} is in units of milliwatts. T, B, and NF represent the temperature (in kelvins), the bandwidth (in hertz), and the noise figure of the receiving unit, respectively.

The channel capacity for a SISO system in additive white Gaussian noise conditions is given by the well-known Shannon capacity equation [31]. MIMO channel capacity is commonly defined by the Foschini capacity equation [10]. In practice, the MIMO channel links at each location also suffer from fast fading based on the value of the K-factor. Hence, the ergodic capacity $\bar{C}$ of the MIMO fading channel for each location is obtained from the ensemble average of the predicted capacity over the distribution of the elements in the $\mathbf{H}$-matrix. When applying OFDM, the data stream is multiplexed into N_f narrowband subcarriers. If the channel is unknown at the transmitter, the channel capacity for a MIMO–OFDM system under frequency-selective fading can be mathematically written as

$$\bar{C} \approx \varepsilon\left\{\frac{1}{N_f}\sum_{j=1}^{N_f}\log_2\det\left(I_{N_R}+\frac{\text{SNR}}{N_T}\mathbf{H}_w(j)\mathbf{H}_w^H(j)\right)\right\} \tag{5}$$

where $\mathbf{H}_w(j)$ represents the frequency response of the correlated MIMO $\mathbf{H}$-matrix ($N_R \times N_T$) for the jth subcarrier, and $(\cdot)^H$ denotes the Hermitian function. Compared to the case of an uncorrelated independent identically distributed Rayleigh fading channel, the theoretic ergodic capacity can be seriously degraded in high correlation conditions [32]. This can occur when the channel K-factor is high, the element spacing is low, or the AS is low. MIMO channel quality is determined by the K-factor, the AoD/AoA spread, the ray geometry, the antenna separation, and the SNR.

IV. TPC

In this section, we consider the impact of TPC in an interference-free hotspot. Power control is performed in terms of the distance between the transmitter and receiver pair. For wireless systems employing AMC and MIMO, the strategy of power control must be carefully considered. Without power control, very high SNR levels are observed by terminals near the AP, often far higher than that required for error-free detection. In [11], the normalization of $\mathbf{H}\mathbf{H}^H$ is explored, and the impact of perfect power control is considered. However, maintaining a high SNR level at the cell edge requires a high AP transmit power. Here, we explore modifications to the "perfect power control" case. However, it should be noted that a detailed analysis of the power control protocol and the implementation of any required modifications is beyond the scope of this paper.

Assuming a nominal transmit power level P_{nom}, DTPC at the AP can be employed on a per peer-station basis (i.e., using a unique power level for each mobile terminal) given knowledge

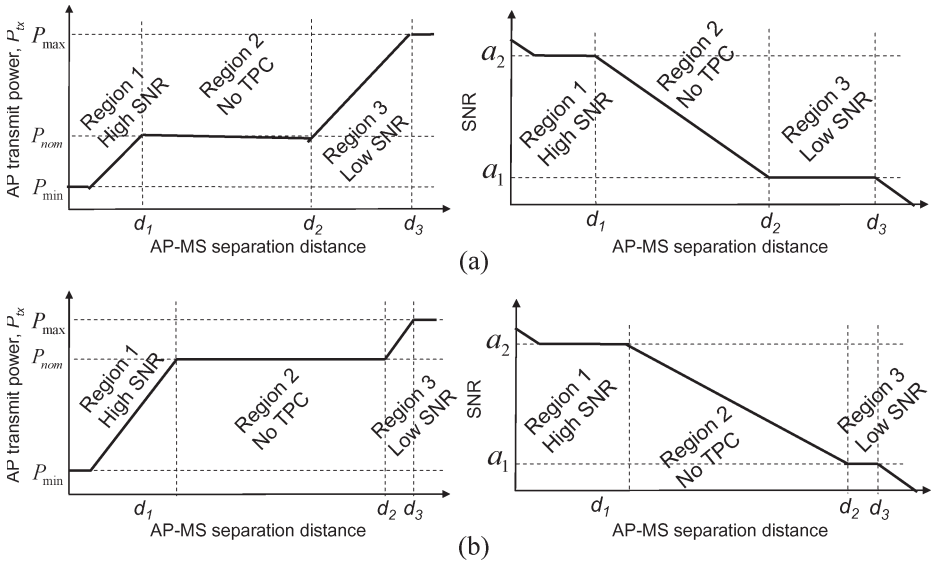

Fig. 4. Transmit power and SNR versus AP–MS distance. (a) Low P_{nom}. (b) High P_{nom}.

of the received SNR per station. Three operating regions can be defined.

1) Region 1 (high SNR): The AP transmit power P_{tx} is reduced in steps until the upper threshold $\mathrm{SNR}_{\max}$ is reached.
2) Region 2 (no power control): The AP uses the nominal transmit power; hence, $P_{\mathrm{tx}}|_{\mathrm{SNR}_{\min}<\mathrm{SNR}\leq\mathrm{SNR}_{\max}} = P_{\mathrm{nom}}$ (see the following discussion for the definition of the variables).
3) Region 3 (low SNR): P_{tx} is increased in steps until the received SNR reaches the minimum threshold $\mathrm{SNR}_{\min}$ or until P_{tx} reaches its maximum value $P_{\mathrm{tx}} = P_{\max}$.

The value of the SNR upper threshold $\mathrm{SNR}_{\max}$ should be set based on the highest required SNR at the terminal (which will normally depend on the highest throughput mode). We introduce the idea of a *nominal* AP transmit power level P_{nom}. If, when this power level is used, the received SNR at the terminal falls between the upper and lower SNR thresholds, then no power control is applied at the AP (region 2). Instead, we allow the AP and terminal to utilize LA to find the most suitable operating mode. Clearly, the value of P_{nom} will have a significant impact on the downlink operating range of the highest throughput modes. Fig. 4 demonstrates this relationship by plotting the SNR and AP transmit power as a function of the AP–MS separation distance. Fig. 4(a) shows the case for a low P_{nom} level. When the minimum power level is reached (extreme left-hand side of the graph), the received SNR at the terminal is shown to rise above the maximum required level, i.e., $\mathrm{SNR}_{\max} = a_2$. As the mobile moves away from the AP, the path loss increases, and to maintain the maximum usable SNR level at the terminal, the AP transmit power rises for this particular terminal until the P_{nom} level is reached (region 1). In Fig. 4, d_1 represents the downlink range for the maximum SNR level. Clearly, a low P_{nom} level results in a much lower value of d_1. As the mobile moves beyond d_1 (into region 2), the transmit power is held at the P_{nom} level until the received SNR drops to the minimum useable value, i.e., $\mathrm{SNR}_{\min} = a_1$; this occurs at distance d_2. Over the range from d_1 to d_2, the AP and mobile terminal link adapt. As the mobile moves further from the AP, the transmit power is increased (region 3) until the maximum value is reached. This creates a constant received SNR level (held at the minimum usable level) up to a separation distance of d_3. Fig. 4(b) compares the DTPC scheme for a high value of P_{nom}. Clearly, using a higher P_{nom} level increases the coverage of the highest throughput mode (d_1 is clearly greater in this case). The point at which LA begins is, thus, further from the AP. It is also noticeable that the region defined by d_2 to d_3 is far smaller (which is desirable since only the minimum performance level can be offered here). A high P_{nom} clearly maximizes the throughput offered to the terminals (and is, thus, well suited to SM), but this comes at the expense of greater transmit power levels.

V. MIMO–OFDM PHY Layer Description

MIMO–OFDM systems offer the potential for a high spectral efficiency, a substantial diversity gain, and a strong immunity to intersymbol interference. The received signal at each subcarrier can be expressed in matrix form as

$$\mathbf{y}_j = \mathbf{H}(j)\mathbf{x}_j + \mathbf{N}_j \tag{6}$$

where $\mathbf{x}_j$ ($N_T \times 1$ vector) and $\mathbf{N}_j$ ($N_R \times 1$ vector) denote the transmitted signal and the noise term at the jth subcarrier, respectively. Since T time slots are used to transmit k symbols, the rate of the space–time code (STC) is defined as $R_{\mathrm{STC}} = k/T$. This type of STC scheme can be defined by an $N_T \times T$ transmission matrix. To clearly demonstrate the tradeoff between the SM and STBC approaches, a range of STC methods is presented, which takes advantage of four transmit antennas (but with different R_{STC}).

A. STBC and Hybrid Scheme

The traditional Alamouti STBC scheme [33] uses two antennas to simultaneously transmit two signals. It has $R_{\mathrm{STC}} = 1$

and offers a similar level of diversity to maximal ratio combining. An STBC scheme using four transmit antennas was proposed by Papadias and Foschini [34]. This pseudo-Alamouti scheme has $R_{\mathrm{STC}} = 1$, but it achieves full spatial diversity since symbols are transmitted over the four antennas. Compared to the traditional Alamouti, the pseudo-Alamouti scheme has partial orthogonality between each pair of transmit antennas.

In the case of a 4×4 MIMO system, a hybrid structure [35], [36] can be used that applies two Alamouti codes and gains some degree of spatial diversity and some degree of SM. The dual Alamouti scheme only has partial orthogonality, as does the pseudo-Alamouti scheme. It offers the same diversity gain as the traditional Alamouti scheme, but it has $R_{\mathrm{STC}} = 2$ due to the addition of SM.

B. MIMO LA With AMC

The IEEE 802.11 and IEEE 802.16 standards define a range of modulation and coding schemes at the PHY layer [4], [5]. Different MIMO system configurations can be applied (with different STC and AMC schemes) to achieve a given link throughput, which can be approximated by Throughput $= D \times (1 - \mathrm{PER})$, where PER represents the packet error rate. $D = N_D N_b R_{\mathrm{FEC}} R_{\mathrm{STC}} / T_s$ represents the transmission date rate, and N_D, N_b, R_{FEC}, and T_s denote the number of data subcarriers, the coded bits per subcarrier, the coding rate, and the OFDM symbol duration, respectively.

In this paper, we assume static fading per packet, and results are averaged over a total of 1000 packets, with 1152 bytes per packet. Forward error correction (FEC) in the form of convolution coding is used, as defined in the 802.11n standard. Minimum mean square error (MMSE) decoding [37] was applied for the SM and hybrid schemes since we focus on illustrating the general trends between SM and STBC, rather than demonstrating the impact of state-of-the-art reception methods. Far lower required SNR values can be achieved for the SM schemes by using more complex receive algorithms [38], [39].

To compare and contrast MIMO performance for a range of quadrature-amplitude modulation (QAM) schemes, Fig. 5 presents the maximum throughput for a range of 20-MHz-wide 4×4 MIMO–OFDM schemes utilizing SM, STBC, and the hybrid scheme with binary phase-shift keying, quaternary phase-shift keying (QPSK), 16QAM, and 64QAM. They all have a coding rate of 3/4. All results were generated for MS location rx #59 [see Fig. 7(a)], which has no dominant ray. The MIMO channels were created by the RTD model, as described in Section II-B. Results show that the SM schemes need a high SNR to achieve the same peak throughput, e.g., for a 36-Mb/s peak throughput, SM requires 25 dB, as compared to only 5 dB for STBC. Throughput can be increased as the modulation scheme and coding rate are increased, but SM then requires an even higher SNR, as shown in Table I.

The mode with the highest throughput (assuming PER $< 10\%$) is selected for each receive location by our "ideal" LA scheme. The selection is described as "ideal" since it relies on simulating the throughput of each mode at each location. As such, the optimum mode is always chosen at each location; however, the algorithm cannot be applied in practice.

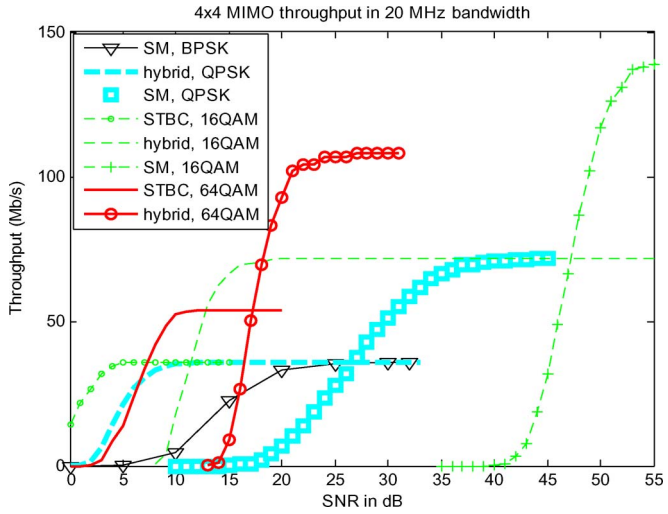

Fig. 5. Throughput for 4×4 MIMO–OFDM in NLoS Rayleigh channel (models detailed in Table I). rx #59: rms AS at AP $= 94.4°$; rms AS at MS $= 34.38°$; rms DS $= 65.05$ ns.

TABLE I
REQUIRED SNR TO ACHIEVE PEAK THROUGHPUT

Configurations	Peak throughput	Required SNR
SM, ¾ rate BPSK	36 Mb/s	25 dB
Hybrid, ¾ rate QPSK	36 Mb/s	10 dB
STBC, ¾ rate 16QAM	36 Mb/s	5 dB
STBC, ¾ rate 64QAM	54 Mb/s	13 dB
SM, ¾ rate QPSK	72 Mb/s	45 dB
Hybrid, ¾ rate 16QAM	72 Mb/s	20 dB
Hybrid, ¾ rate 64QAM	108 Mb/s	27 dB
SM, ¾ rate 16QAM	144 Mb/s	60 dB

Channel conditions: RMS AS at AP = 94.4 degrees; RMS AS at MS = 34.38 degrees; RMS DS = 65.05 ns.

VI. NUMERICAL RESULTS

In this section, a set of simulation results that include PER versus SNR graphs, link throughput versus SNR predictions, and hotspot area coverage is presented. A new set of ten PHY layer candidates is modeled (as shown in Fig. 6), with each scheme operating with a 40-MHz bandwidth [40]. The schemes include five SM candidates, three hybrid STBC/SM schemes, and two STBC candidates. To evaluate area coverage, we define a maximum PER of 10% [41]. If all of our chosen schemes exceed this PER, then the point is assumed to lie in outage.

A single AP was deployed toward the top of a lamppost at a height of 5 m (above ground level). The lamppost was located in the center of a 400 m $\times$ 400 m simulation grid. Omnidirectional antennas were horizontally arranged in the form of a ULA with $\lambda/2$ separations. The AP and MS array elements were aligned to lie north-to-south. The mobile locations were uniformly deployed over a square grid with a 5-m spacing. A carrier frequency of 5.2 GHz was used, and the DTPC algorithm discussed in Section IV was applied with $\mathrm{SNR}_{\max} = 30$ dB, $\mathrm{SNR}_{\min} = 15$ dB, $P_{\mathrm{nom}} = 30$ dBm, and $P_{\mathrm{tx,max}} = 40$ dBm. The LA algorithm attempts to achieve the highest link throughput without exceeding $\mathrm{SNR}_{\max}$ and $P_{\mathrm{tx,max}}$. All other PHY layer parameters, unless explicitly stated, are assumed to follow the IEEE 802.11a/n standard. The system noise temperature

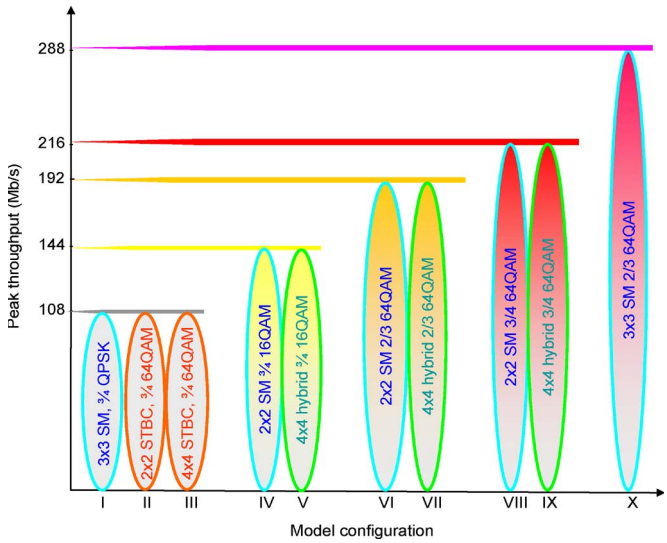

Fig. 6. System configurations at the PHY layer (in a 40-MHz bandwidth).

was 290 K, and a noise figure of 3 dB [42] was used. The PER for each of the MIMO–OFDM PHY layer schemes was simulated using the SNR and the MIMO channel data from the RTD model for each MS location.

MIMO communication capacity is dependent on channel phenomenology, and the singular value distribution is a useful tool for understanding the expected MIMO performance [43]. Fig. 7(a) presents the distribution of the mean reciprocal condition number (RCN) [44] (measured over 1000 3×3 MIMO channels), where the instantaneous RCN is given by $\min(\mu)^2 / \max(\mu)^2$, and μ represents the vector of singular values from each matrix $\mathbf{H}\mathbf{H}^H$. Small values of the RCN tend to occur in locations with strong LoS (and, hence, high K-factor). The assumed relationship between DS and AS in the TGn802.11n model results in larger AS values and, hence, an overprediction of capacity in the outdoor hotspot. This is particularly noticeable in strong LoS regions (i.e., in the same street as the AP), as shown in Fig. 7(b). Fig. 7(c) shows the service coverage for the 3×3 SM-based MIMO–OFDM system (mode I) in the simulation area. In these cases, a high degree of spatial correlation can occur, and this can have a detrimental effect on MIMO system performance. In contrast, low correlated MIMO channels tend to have a large RCN. Given that the SM schemes under consideration have a low immunity to high correlation values, frequent gaps in the predicted coverage area can be seen. It is also evident that service cannot be reliably provided when the mobile moves close to the AP, since a very strong LoS component exists, and this creates high spatial correlation and, thus, low rank in the resulting $\mathbf{H}\mathbf{H}^H$ matrix. For such cases, although the SNR is high, the 3×3 SM scheme is unable to meet the 10% PER target. From analysis of the grid shown in Fig. 7(c), we conclude that at the PHY layer, this particular SM scheme cannot operate with a PER less than 10% for locations with a low RCN or a low SNR.

Each of the ten MIMO–OFDM schemes in Fig. 6 is now modeled using site-specific channel data (as discussed in Section II-B) extracted for every MS–AP link in the service area. A total of 6000 MS–AP links were analyzed per

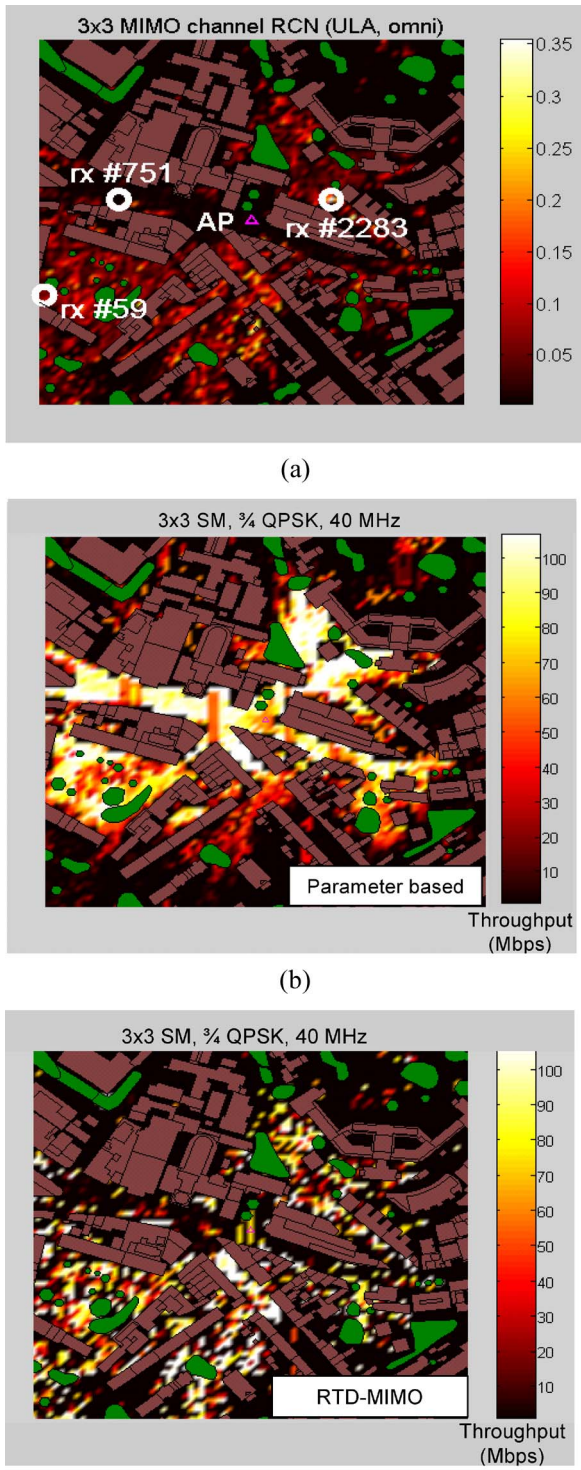

Fig. 7. Grid plots. (a) RCN. (b) Throughputs based on TGn802.11n assumptions. (c) Throughputs based on ray tracing.

scheme, resulting in 60 000 individual PHY layer simulation studies. For each study, 1000 data packets were simulated (each 1152 bytes in length) to determine the expected PER and throughput. In total, this required the simulation of 6 million data packets. Fig. 8 plots the area coverage versus throughput for each of the ten MIMO–OFDM schemes. Clearly, in all cases, throughput is shown to drop as the PER increases.

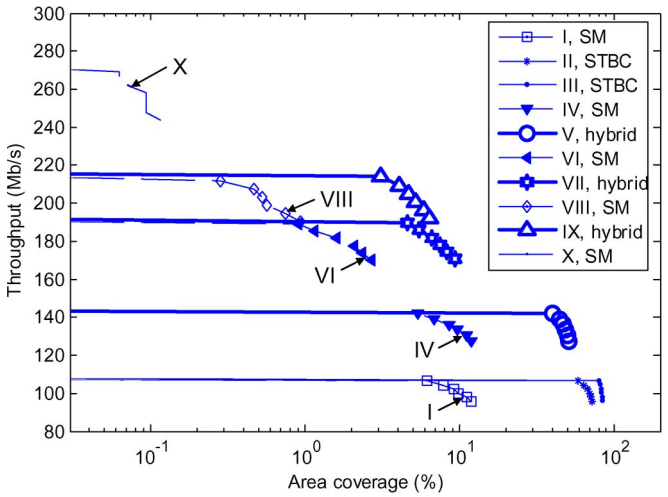

Fig. 8. Area coverage versus throughput for each of the MIMO configurations.

TABLE II
% AREA COVERAGE BY OPERATING MODE AND LA

PHY mode		% area covered by mode (PER < 10%)	Maximum data rate	% area covered by LA
STBC	II	72.00%	108 Mb/s	16.42%
	III	84.99%	108 Mb/s	32.74%
Hybrid	V	50.19%	144 Mb/s	40.76%
	VII	8.40%	192 Mb/s	2.25%
	IX	5.96%	216 Mb/s	5.90%
SM	I	11.11%	108 Mb/s	0.00%
	IV	11.14%	144 Mb/s	1.00%
	VI	2.34%	192 Mb/s	0.84%
	VIII	0.72%	216 Mb/s	0.03%
	X	0.06%	288 Mb/s	0.06%

Given our maximum 10% PER outage criteria, STBC modes II and III achieve a maximum coverage area of 72% and 85%, respectively. Both modes utilize 64QAM, which, in the case of STBC, can be successfully deployed. SM modes I, IV, VI, VIII, and X achieve a maximum area coverage of 11.11%, 11.14%, 2.34%, 0.72%, and 0.06%, respectively. Clearly, SM results in very limited coverage (peaking at only 11.14%) of the service area. For SM, as the modulation order increases, the percentage coverage area is shown to decrease. The highest peak rate SM scheme (mode X using 64QAM) is almost never used. The use of the hybrid algorithm brings a significant increase in area coverage. Hybrid modes V, VII, and IX offer a maximum coverage area of 50.19%, 8.4%, and 5.96%, respectively. The most successful hybrid mode uses 16QAM modulation. Compared to pure SM, in the hybrid case, the area coverage for 64QAM is much improved. These coverage data are summarized in Table II, where the maximum area coverage for each scheme is quoted against its peak data rate.

Table II quotes the percentage area coverage for each scheme after application of the ideal LA algorithm. STBC modes II and III are chosen for 16.42% and 32.74% of locations, respectively. Overall, STBC schemes are chosen for approximately 50% of covered locations. Hybrid mode V is selected for 40.76% of covered locations, making it the most successful mode of those studied in this paper. Overall, hybrid schemes are chosen for

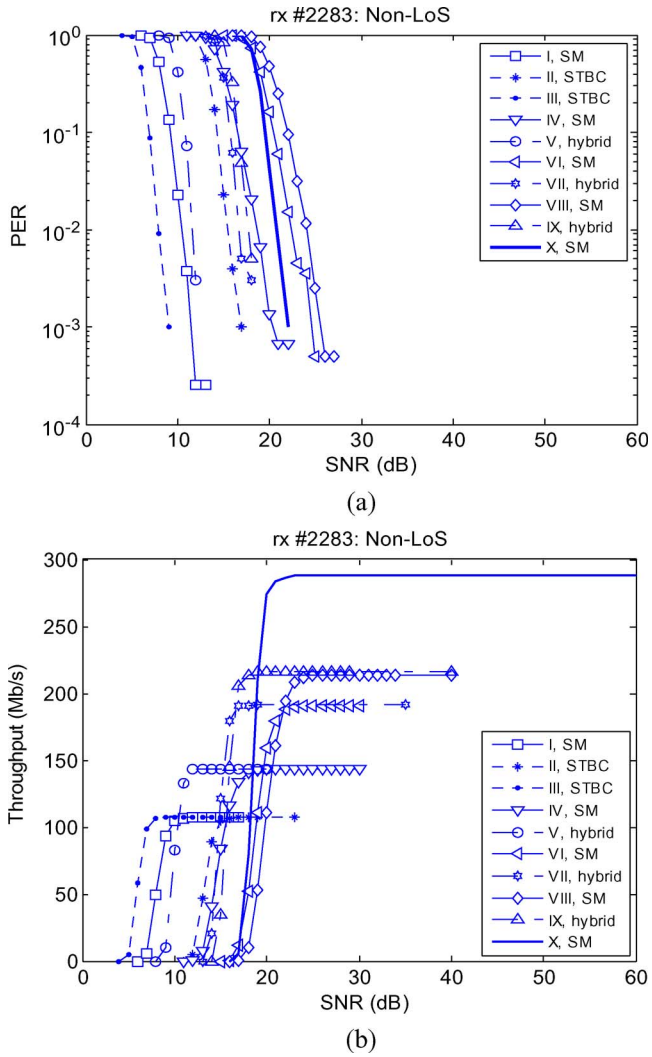

Fig. 9. NLoS analysis for rx #2283. (a) PER. (b) Throughput (K-factor = 0.75 dB; rms AS at AP = 49.2°; rms AS at MS = 140.4°; rms DS = 110.8 ns).

approximately 48% of covered locations. SM modes IV and VI are chosen for 1.00% and 0.84% of locations, respectively. Overall, SM schemes are chosen for approximately 2% of locations. Interestingly, although SM mode I is usable at 11.11% of locations, it is never chosen by the ideal LA algorithm. Given that this mode offers a peak rate of only 108 Mb/s, we note that the 64QAM STBC modes offer a higher throughput at all SNR values.

Figs. 9 and 10 present the PER and throughput curves for all ten schemes for the two particular test cases shown in Fig. 7(a), namely NLoS (e.g., rx #2283) and LoS (e.g., rx #751). Results indicate that mode III (4×4 STBC) offers a powerful diversity gain for both rx #2283 and rx #751. It can be seen that mode I (3×3 SM with 3/4 rate QPSK) offers the second lowest PER for rx #2283 [Fig. 9(a)], but it has the second highest PER for rx #751, as shown in Fig. 10(a). For rx #2283, a 288-Mb/s throughput is achievable using mode X (3×3 SM with 2/3 rate 64QAM) at a required SNR of around 23 dB [Fig. 9(b)]. In contrast, such high throughputs are never obtained at rx #751 for practical SNR values (i.e., less than 30 dB), and the maximal peak throughput is 216 Mb/s [Fig. 10(b)]. Generally, if the

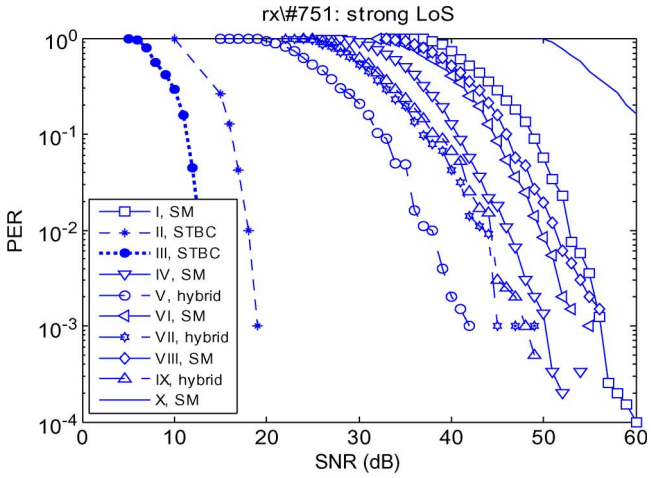

(a)

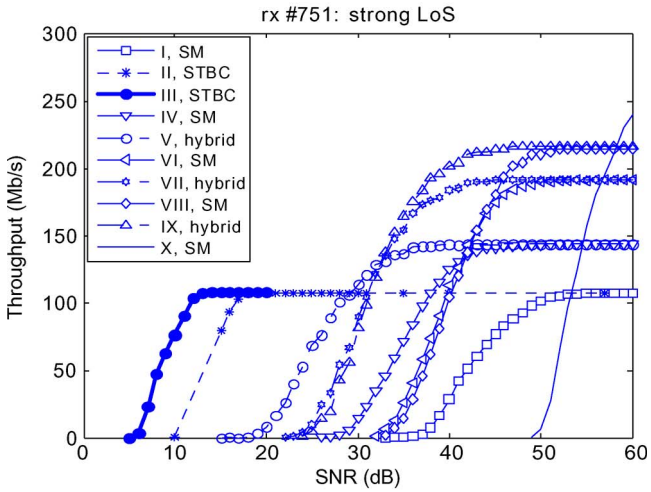

(b)

Fig. 10. LoS analysis for rx #751. (a) PER. (b) Throughput (K-factor = 10 dB; rms AS at AP = 11.8°; rms AS at MS = 4°; rms DS = 5.6 ns).

channel is NLoS, then the required SNR is far lower than the corresponding strong LoS case. For example, at rx #2283, mode V (a 4 × 4 hybrid) and mode IV (2 × 2 SM) can operate at SNRs of 12 and 19 dB, respectively, to provide a peak transmission rate of 144 Mb/s. At rx #751, the required SNR increases to 36 and 43 dB for these two modes. Results also show that at peak rates in excess of 108 Mb/s, the hybrid schemes have a lower required SNR than the SM schemes for a given peak throughput. Finally, in Fig. 10(a), it is interesting to note that the three best modes (III, II, and V) for this NLoS test point correspond to those most chosen by the LA algorithm (see Table II).

As previously mentioned, higher order modulation schemes using SM need more transmit power to operate at a low PER. STBC offers a diversity gain, but this comes at the expense of a lower peak capacity. In practice, high throughput at a low SNR (and low receive complexity) is desirable. Previous results from Figs. 7(c) and 8 indicate that SM (using MMSE detection) cannot be used in the vast majority of locations. An adaptive system is attractive to switch between a range of different MIMO modes as required. Table III demonstrates that high capacity (up to 288 Mb/s) and good geographic coverage can be combined.

TABLE III
TRANSMIT DATA RATE AND COVERAGE BY LA

Maximal data rate	Percentage of users
288 Mb/s	0.06%
216 Mb/s	6.15%
192 Mb/s	9.24%
144 Mb/s	51.15%
108 Mb/s	87.83%
failed	12.17%

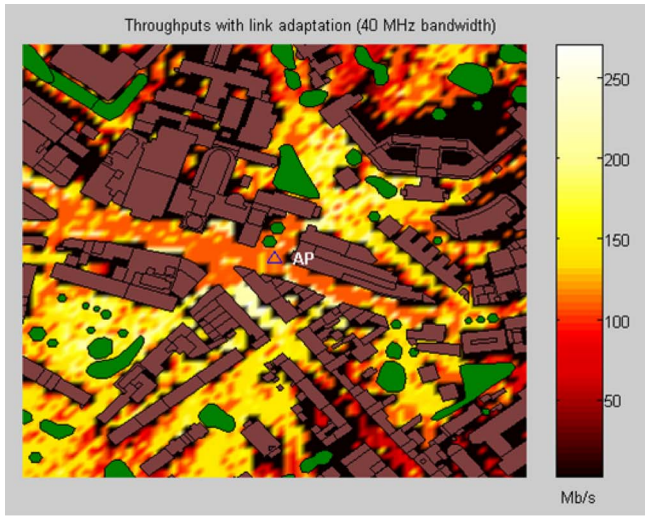

(a)

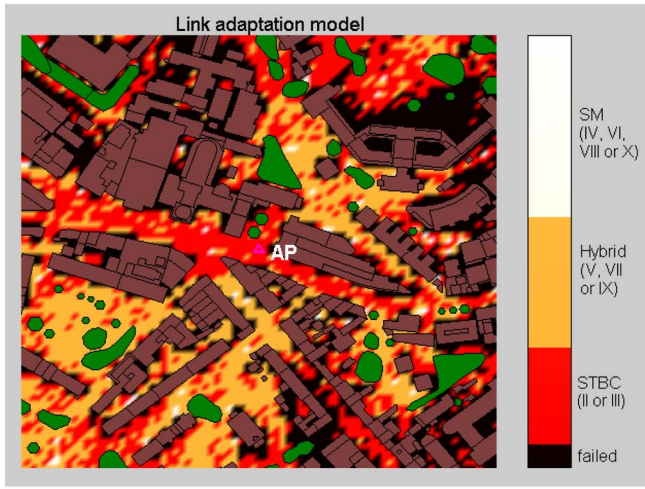

(b)

Fig. 11. Grid plots. (a) Achievable maximal throughput. (b) LA model.

In summary, 6.15% of locations in this test area can support 216 Mb/s or better, 9.24% can support 192 Mb/s or better, 51.15% can support 144 Mb/s or better, and 87.83% can support 108 Mb/s or better. Hence, 12.17% of locations remain in outage. In practice, a range of lower peak rate modes would be used to cover these regions.

Fig. 11(a) shows the maximum predicted throughput at each point in the test location, whereas Fig. 11(b) shows the selected mode (by group). It can be seen that SM schemes are only chosen in areas with rich multipath scatter [see Fig. 7(a)] and a high SNR. In general, both the SM and hybrid schemes are

better suited to NLoS regions. The hybrid schemes can be used to capture the diversity gain. As such, the 4×4 hybrid mode offers coverage in many more locations than the standard SM schemes (as confirmed by Table II). STBC is clearly preferred in LoS locations (i.e., in the same street as the AP) and for distant locations near the cell edge (where the SNR is low). We note that high data rates from 108 to 288 Mb/s are achieved, although LA (even as the user moves over small distances) is vital to ensure optimum performance.

VII. Conclusion

This paper has presented a detailed study of urban MIMO–OFDM performance based on theoretic evaluations and a unique set of ray-tracing/simulation studies. The combination of area-wide link-level simulations using MIMO channel data from an urban ray-tracing propagation model provides unique insights into system performance.

SM, combined with higher order modulation, was shown to increase the peak link throughput if full rank channels and a high SNR are available. STBC was shown to offer strong diversity gains at a low SNR but could not increase the link throughput unless combined with AMC (see Table I).

A key focus of this paper was the comparison of SM with STBC and hybrid SM/STBC schemes. Results showed that there were fundamental tradeoffs between the use of STBC and SM. STBC (which offers a strong diversity gain) was more suitable when the mobile was located in LoS to the AP (where the channel rank is low) or placed toward the cell edge (where the SNR is low). SM schemes worked well in locations with a high SNR and rich multipath scatter (indicated by a large RCN). For NLoS regions, the hybrid STBC/SM scheme was shown to greatly enhance the area coverage while also improving the PER versus SNR performance. Interestingly, no MIMO scheme was able to effectively operate over the entire service area.

Results clearly demonstrate the need for suitable MIMO-oriented LA strategies that take into account the wide range of channel conditions encountered in practice (both the SNR and rank). LA should be used to select the type of MIMO algorithm, the particular modulation and coding scheme, and the number of antenna elements at both ends of the link. For our test environment, results showed that approximately 2% of covered locations selected SM, 48% selected hybrid operation, and 50% selected STBC. In total, 87.83% of locations were covered with a data rate of 108 Mb/s or better.

Acknowledgment

The authors would like to thank Dr. M. Sandell for his valuable technical input.

References

[1] *Strategy for the Future Use of the Radio Spectrum in the UK (2002)*, 2002, London, U.K: Radio Commun. Agency.

[2] A. Paulraj, R. Nabar, and D. Gore, *Introduction to Space–Time Wireless Communications*. Cambridge, U.K.: Cambridge Univ. Press, 2003.

[3] R. Prasad and R. van Nee, *OFDM for Wireless Multimedia Communications*. Norwood, MA: Artech House, 2000.

[4] *Draft Supplement to Standard for LAN/MAN Part 11: MAC & PHY Specifications*, IEEE Std. P802.11a/D7.0, Jul. 1999.

[5] *Part 16: Air Interface for Fixed Broadband Wireless Access Systems*, IEEE Std. 802.16-2004, Oct. 2004.

[6] H. Sampath, S. Talwar, J. Tellado, V. Erceg, and A. Paulraj, "A fourth-generation MIMO–OFDM broadband wireless system: Design performance, and field trial results," *IEEE Commun. Mag.*, vol. 40, no. 9, pp. 143–149, Sep. 2002.

[7] A. Zelst and T. Schenk, "Implementation of a MIMO OFDM-based wireless LAN system," *IEEE Trans. Signal Process.*, vol. 52, no. 2, pp. 483–494, Feb. 2004.

[8] *Antenna Array Technology and MIMO Systems*, Mar. 2004. OFCOM Doc.8366CR2. [Online]. Available: http://www.ofcom.org.uk/research/technology/ses/ses2003-04/ay4476b

[9] Y. Bian, A. Nix, E. Tameh, and J. McGeehan, "High throughput MIMO–OFDM WLAN for urban hotspots," in *Proc. IEEE VTC—Fall*, Sep. 2005, vol. 1, pp. 296–300.

[10] G. Foschini, "Layered space–time architecture for wireless communication in a fading environment when using multi-element antennas," *Bell Labs Tech. J.*, vol. 1, no. 2, pp. 41–59, 1996.

[11] L. Dong, H. Ling, and R. Heath, Jr., "Multiple-input multiple-output wireless communication systems using antenna pattern diversity," in *Proc. IEEE GLOBECOM*, Nov. 2002, vol. 1, pp. 997–1001.

[12] S. Catreux, V. Erceg, D. Gesbert, and R. W. Heath, Jr., "Adaptive modulation and MIMO coding for broadband wireless data networks," *IEEE Commun. Mag.*, vol. 40, no. 6, pp. 108–115, Jun. 2002.

[13] R. Heath, Jr. and A. Paulraj, "Switching between diversity and multiplexing in MIMO systems," *IEEE Trans. Commun.*, vol. 53, no. 6, pp. 962–968, Jun. 2005.

[14] A. Forenza, A. Pandharipande, H. Kim, and R. W. Heath, Jr., "Adaptive MIMO transmission scheme: Exploiting the spatial selectivity of wireless channels," in *Proc. IEEE VTC—Spring*, May 2005, vol. 5, pp. 3188–3192.

[15] A. Forenza, M. Airy, M. Kountouris, R. W. Heath, Jr., D. Gesbert, and S. Shakkottai, "Performance of the MIMO downlink channel with multi-mode adaptation and scheduling," in *Proc. IEEE Workshop Signal Process. Adv. Wireless Commun.*, Jun. 2005, pp. 695–699.

[16] L. Zheng and D. Tse, "Diversity and multiplexing: A fundamental tradeoff in multiple-antenna channels," *IEEE Trans. Inf. Theory*, vol. 49, no. 5, pp. 1073–1096, May 2003.

[17] *IEEE 802.11 Wireless LANs, TGn Channel Models*, IEEE Std. 802.11-03/940r4, May 2004.

[18] J. Kermoal, L. Schumacher, P. Mogensen, and K. Pedersen, "Experimental investigation of correlation properties of MIMO radio channels for indoor picocell scenario," in *Proc. IEEE VTC—Fall*, Sep. 2000, vol. 1, pp. v14–v21.

[19] L. Schumacher, K. Pedersen, and P. Mogensen, "From antenna spacings to theoretical capacities—Guidelines for simulating MIMO systems," in *Proc. IEEE PIMRC*, Sep. 2002, vol. 2, pp. 587–592.

[20] P. Soma, D. Baum, V. Erceg, R. Krishnamoorthy, and A. Paulraj, "Analysis and modelling of multiple-output (MIMO) radio channel based on outdoor measurements conducted at 2.5 GHz for fixed BWA applications," in *Proc. IEEE ICC*, Apr. 2002, vol. 1, pp. 272–276.

[21] H. Ozcelik, M. Herdin, W. Weichselberger, J. Wallace, and E. Bonek, "Deficiencies of 'Kronecker' MIMO radio channel model," *Electron. Lett.*, vol. 39, no. 16, pp. 1209–1210, Aug. 2003.

[22] W. Weichselberger, M. Herdin, H. Ozcelik, and E. Bonek, "A stochastic MIMO channel model with joint correlation of both link ends," *IEEE Trans. Wireless Commun.*, vol. 5, no. 1, pp. 90–100, Jan. 2006.

[23] S. Wyne, A. Molisch, P. Almers, G. Eriksson, J. Karedal, and F. Tufvesson, "Statistical evaluation of outdoor-to-indoor office MIMO measurements at 5.2 GHz," in *Proc. IEEE VTC—Spring*, May 2005, vol. 1, pp. 146–150.

[24] C. Oestges, H. Ozcelik, and E. Bonek, "On the practical use of analytical MIMO channel models," in *Proc. IEEE Antennas Propag. Symp.*, Jul. 2005, vol. 3B, pp. 406–409.

[25] K. Ng, E. Tameh, A. Doufexi, M. Hunukumbure, and A. Nix, "Efficient multi-element ray tracing with site specific comparisons using measured MIMO channel data," *IEEE Trans. Veh. Technol.*, vol. 56, no. 3, pp. 1019–1032, May 2007.

[26] E. Tameh, A. Nix, and M. Beach, "A 3-D integrated macro and microcellular propagation model, based on the use of photogrammetric terrain and building data," in *Proc. IEEE VTC*, May 1997, vol. 3, pp. 1957–1961.

[27] L. Dong, H. Choo, R. Heath, Jr., and H. Ling, "Simulation of MIMO channel capacity with antenna polarization diversity," *IEEE Trans. Wireless Commun.*, vol. 4, no. 4, pp. 1869–1873, Jul. 2005.

[28] A. Forenza and R. Heath, Jr., "Benefit of pattern diversity via two-element array of circular patch antennas in indoor clustered MIMO channels," *IEEE Trans. Commun.*, vol. 54, no. 5, pp. 943–954, May 2006.
[29] M. Stege, J. Jelitto, M. Bronzel, and G. Fettweis, "A multiple input-multiple output channel model for simulation of Tx and Rx-diversity wireless systems," in *Proc. IEEE VTC—Fall*, Sep. 2000, vol. 2, pp. 833–839.
[30] A. Molisch, "A generic model for MIMO wireless propagation channels in macro and microcells," *IEEE Trans. Signal Process.*, vol. 52, no. 1, pp. 61–71, Jan. 2004.
[31] C. Shannon, "A mathematical theory of communication," *Bell Labs Tech. J.*, vol. 27, pp. 379–423, Jul.–Oct. 1948.
[32] D.-S. Shiu, G. Foschini, M. Gans, and J. Kahn, "Fading correlation and its effect on the capacity of multi-element antenna systems," *IEEE Trans. Commun.*, vol. 48, no. 3, pp. 502–513, Mar. 2000.
[33] M. Alamouti, "A simple transmit diversity technique for wireless communications," *IEEE J. Sel. Areas Commun.*, vol. 16, no. 8, pp. 1451–1458, Oct. 1998.
[34] C. Papadias and G. Foschini, "A space–time coding approach for systems employing four transmit antennas," in *Proc. IEEE ICASSP*, May 2001, vol. 4, pp. 2481–2484.
[35] M. Debbah, B. Muquet, M. Courville, M. Muck, S. Simoens, and P. Loubaton, "A MMSE successive interference cancellation scheme for a new adjustable hybrid OFDM system," in *Proc. IEEE VTC—Spring*, May 2000, vol. 2, pp. 745–749.
[36] E. Onggosanusi, A. Dabak, and T. Schmidl, "High rate space–time block coded scheme: Performance and improvement in correlated fading channels," in *Proc. IEEE Wireless Commun. Netw. Conf.*, Mar. 2002, vol. 1, pp. 194–199.
[37] A. Naguib, N. Seshadri, and A. Calderbank, "Applications of space–time block codes and interference suppression for high capacity and high data rate wireless system," in *Conf. Rec. 32nd Asilomar Conf. Signals, Syst., Comput.*, Nov. 1998, vol. 2, pp. 1803–1810.
[38] R. Piechocki, C. Andrieu, C. Vithange, and J. McGeehan, "Joint space–time trellis code detection and MIMO equalization via particle filtering," in *Proc. 1st Int. Symp. IEEE Wireless Commun. Syst.*, Sep. 2004, pp. 357–361.
[39] D. Gesbert, "Robust linear MIMO receivers: A minimum error-rate approach," *IEEE Trans. Signal Process.*, vol. 51, no. 11, pp. 2863–2871, Nov. 2003.
[40] [Online]. Available: http://dailywireless.org/modules.php?name=News&file=article&sid=3491&src=rss09
[41] [Online]. Available: http://games.dlink.com/products/resource.asp?pid=333&rid=1185
[42] [Online]. Available: http://www.satsig.net/noise.htm
[43] D. Bliss, A. Chan, and N. Chang, "MIMO wireless communication channel phenomenology," *IEEE Trans. Antennas Propag.*, vol. 52, no. 8, pp. 2073–2082, Aug. 2004.
[44] V. Nangia and K. Baum, "Experimental broadband OFDM system: Field results for OFDM and OFDM with frequency domain spreading," in *Proc. IEEE VTC—Fall*, Sep. 2002, vol. 1, pp. 223–227.

Yan Q. Bian received the B.Eng. degree from Nanjing University of Post and Telecommunication, Nanjing, China, in 1986 and the Ph.D. degree from the University of Bristol, Bristol, U.K., in 2003.

From 1986 to 1997, she was with the Ministry of Post and Telecommunications, China, where she became a Project Manager. She joined the University of Bristol in 1998. She was a Research Engineer with Toshiba Research Europe Ltd., Bristol, in 2001. She is currently a Research Fellow with the Centre for Communications Research, University of Bristol. Her research interests include wireless LANs, broadband wireless access networks, applications of MIMO, interference cancellation, channel estimation, and relay transmission.

Andrew R. Nix received the B.Eng. and Ph.D. degrees from the University of Bristol, Bristol, U.K., in 1989 and 1993, respectively.

He is currently a Professor of wireless communication systems with the University of Bristol. He has managed numerous European Union, Engineering and Physical Sciences Research Council, and Department of Trade and Industry funded projects. He is the author or coauthor of more than 250 papers published in international journals and conference proceedings. His main research interests include broadband wireless communications, radiowave propagation modeling, cellular network optimization, and advanced digital modulation/reception techniques.

Eustace K. Tameh received the B.Sc. degree (with honors) in electronic engineering and mathematics from Keele University, Staffordshire, U.K., in 1994 and the Ph.D. degree in wide-area propagation prediction and planning from the University of Bristol, Bristol, U.K., in 1998.

He joined the University of Bristol in 1994, where he became a Research Associate in 1997, working on research projects on propagation modeling and cellular network design. In 2006, he joined ProVision Communication Technologies Ltd., Bristol, where he leads the development of a range of RF planning tools. His current research interests include the development of novel planning techniques for broadband and next-generation wireless networks.

Joseph P. McGeehan received the B.Eng. and Ph.D. degrees in electrical and electronic engineering and the D.Eng. degree for his significant contribution to the field of mobile communications research from the University of Liverpool, Liverpool, U.K., in 1967, 1971, and 2003, respectively.

He is currently a Professor of communications engineering and the Director of the Centre for Communications Research, University of Bristol, Bristol, U.K. He is concurrently the Managing Director of Toshiba Research Europe Ltd., U.K. He has been actively researching spectrum-efficient mobile radio communication systems since 1973 and has pioneered work in many areas, including linear modulation, linear power amplifiers, smart antennas, propagation modeling, and phase-locked loops.

Prof. McGeehan is a Fellow of the Royal Academy of Engineering and the Institution of Electrical Engineers. He has served on numerous international committees and standards bodies and was advisor to the U.K.'s first DTI/MOD "Defense Spectrum Review Committee" in the late 1970s. He was the joint recipient of the IEEE Vehicular Technology Transactions Neal Shepherd Memorial Award (for work on smart antennas) and the *IEE Proceedings* Mountbatten Premium (for work on satellite tracking and frequency control systems). In 2004, he was made a Commander of the Order of the British Empire on the Queen's Birthday Honors List for services to the communications industry.